OPEN

Correspondence and
requests for materials
should be addressed to
Y.D. (yyduan@
tsinghua.edu.cn)

A New Route for Unburned Carbon Concentration Measurements Eliminating Mineral Content and Coal Rank Effects

Dong Liu, Yuan-Yuan Duan, Zhen Yang & Hai-Tong Yu

Key Laboratory of Thermal Science and Power Engineering of Ministry of Education, Beijing Key Laboratory for CO_2 Utilization and Reduction Technology, Tsinghua University, Beijing 100084, China.

500 million tons of coal fly ash are produced worldwide every year with only 16% of the total amount utilized. Therefore, potential applications using fly ash have both environmental and industrial interests. Unburned carbon concentration measurements are fundamental to effective fly ash applications. Current on-line measurement accuracies are strongly affected by the mineral content and coal rank. This paper describes a char/ash particle cluster spectral emittance method for unburned carbon concentration measurements. The char/ash particle cluster spectral emittance is predicted theoretically here for various unburned carbon concentrations to show that the measurements are sensitive to unburned carbon concentration but insensitive to the mineral content and coal rank at short wavelengths. The results show that the char/ash particle cluster spectral emittance method is a novel and promising route for unburned carbon concentration on-line measurements without being influenced by mineral content or coal rank effects.

The world currently produces 500 million tons of coal fly ash each year[1]. This fly ash is quite dangerous because of its high toxic element content and which can affect people's health and cause genetic mutations[2–7]. Therefore, fly ash is collected and either utilized or disposed of in landfills at significant costs[8,9]. Currently only 16% of the total fly ash is utilized worldwide[1] which means that significant disposal costs are charged to the power companies and, thus, to consumers. Therefore, research on potential applications to use fly ash has both environmental and industrial interests.

The high specific surface area makes fly ash a low cost adsorbent for coal fired flue gas and waste water treatment[1]. Intrinsic fly ash and activated carbon and zeolite generated from fly ash have been used to capture CO_2[10–17] and to adsorb SO_x[18], NO_x[18] and mercury[19–25] in flue gas and to remove toxic metals and organic compounds[26–29] from waste water. The geotechnical properties (specific gravity, permeability and consolidation), make fly ash a promising construction material[1]. Investigations have shown that the unburned carbon component in fly ash is important for its applications[1,10,18,21,22,25]. Fly ash must have a low unburned carbon content when used as a construction material in the cement industry since the unburned carbon undesirably adsorbs the air entraining agents added to prevent cement crack formation[10]. The unburned carbon concentrations in fly ash have increased dramatically since utility boilers have been using low NO_x burners to meet the Clean Air Act NO_x emission requirements. As a result the unburned carbon concentrations in fly ash range from 2% to 20%, which restricts fly ash use as a construction material. However, the higher unburned carbon concentrations make fly ash a more efficient adsorbent for flue gas and waste water treatment[18,21,22,25] since the unburned carbon contributes much of the surface area to fly ash. Therefore, unburned carbon concentration measurements are of fundamental importance in fly ash applications.

The standard unburned carbon concentration measurement method is the loss-on-ignition test. Sample fly ash is removed from the exhaust, and then oxidized at 850°C for several hours in a muffle furnace. The weight loss is the unburned carbon weight. However, the analytical process takes up to 24 hours so it cannot be used on-line as a real time monitor of the unburned carbon concentration and the boiler working status. The photo-acoustic effect has also been used to measure unburned carbon concentrations[30,31]. However, the fly ash sample has to be ground prior to measurements to reduce the carbon particle size effect[30], so this method cannot be used on-line. On-line
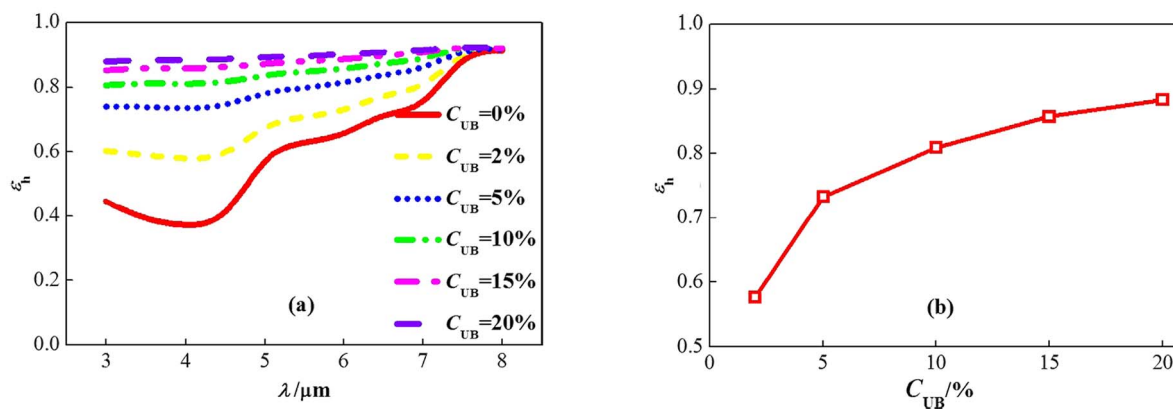
Figure 1 | Spectral emittance of Shenhua coal char/ash particle clusters with C_{UB} ranging from 0 to 20%. (a) Effects of C_{UB} on the spectral emittance. (b) Spectral emittance at 4 μm.

methods include microwave absorption[32,33], optical dispersion-reflection[34,35], laser-induced breakdown spectroscopy[36,37] and infrared emissions[38]. The measurement accuracies of these methods are strongly affected by the mineral content and the coal rank[36,37,39]. The relative errors can be as high as 30% for the microwave absorption method[32], 50% for the optical dispersion-reflection method[34], and 40% for the laser-induced breakdown spectroscopy method[37].

This paper describes a char/ash particle cluster spectral emittance method to measure the unburned carbon concentration. The char/ash particle cluster spectral emittance is shown theoretically to be sensitive to the unburned carbon concentrations and insensitive to the mineral content and coal rank at short wavelengths. Thus, the char/ash particle cluster spectral emittance method is a novel and promising route for on-line unburned carbon concentration measurements that are insensitive to the mineral content and coal rank effects.

Results

Unburned carbon concentration effect. Figure 1(a) shows the spectral emittance of char/ash particle clusters of a typical Chinese bituminous coal, Shenhua coal, produced in Shanxi Province, with unburned carbon concentrations, C_{UB}, ranging from 0 (pure fly ash cluster) to 20%. The char and ash particle sauter diameters were both 9 μm, the particle volume fraction was 0.2 and the mineral content are summarized in Table 1[40].

The spectral emittance is low at wavelengths below 4 μm, increases sharply at wavelengths between 4 and 8 μm, and approaches unity at 8 μm for the pure fly ash cluster and the char/ash clusters with C_{UB} below 5%. The spectral emittance is almost constant within the whole wavelength range for the char/ash particle clusters with C_{UB} above 10%. This evident grey nature agrees with spectral emittance experimental data for devolatilized carbon-rich char particle clusters[41]. The spectral emittance is close to unity and does not change with C_{UB} at wavelengths above 7 μm. However, the spectral emittance is strongly sensitive to C_{UB} at wavelengths below 4 μm, which implies that C_{UB} can be determined by measuring the char/ash particle cluster spectral emittance at a low wavelength. The char/ash particle cluster spectral emittance at 4 μm is plotted versus C_{UB} in figure 1(b). The slope is higher for C_{UB} below 10%; thus, the char/ash particle cluster spectral emittance method tends to be more

accurate for measuring the unburned carbon concentration in fly ash with lower C_{UB}.

Mineral content and coal rank effects. Current on-line measurement methods are strongly affected by the mineral content and coal rank[32–38]. These effects are investigated here for the char/ash particle cluster spectral emittance method. Figure 2(a) compares the spectral emittance at 4 μm for char/ash particle clusters of Shenhua coal and another typical Chinese bituminous coal, Yankuang coal, produced in Shandong Province, which have different mineral content as summarized in Table 1[42]. The average relative difference of the spectral emittance for these two coal char/ash clusters is 0.4%, which shows that the mineral content has little effect on the char/ash particle cluster spectral emittance and, thus, on the unburned carbon concentration measurements using the char/ash particle cluster spectral emittance method.

For low rank coals such as sub-bituminous coal and lignite, the fly ash has more calcium oxide and less silica than high rank coals[1]. The unburned carbon content also has larger particles and higher vitrinite maceral components which are more porous than inertinite components; thus, lower rank coals have higher porosities[43]. As explained above, the mineral content has little effect on the measurements. Since the carbon-rich extracts separated from the fly ash mineral content for low rank coals also typically have carbon concentrations of about 75%[44,45], the carbon concentration of a single char particle and the number of char and ash particles remained unchanged. The porosity of a single char particle, however, increased from 50% to 75%, and the particle diameter of a single char particle increased from 9 μm to 11 μm accordingly for the Shenhua coal char/ash clusters to investigate the effect of coal rank. The average relative difference of the spectral emittance before and after changing the porosity and particle diameter is 2.5% as illustrated in figure 2(b), which shows that the coal rank has little effect on the char/ash particle cluster spectral emittance and, thus, on the unburned carbon concentration measurements.

Implications. The char/ash particle cluster spectral emittance depends on the optical depth, τ, the phase function, $\Phi(\mu.\mu')$, and the scattering albedo, ω, as shown in equation (1). Char/ash particle clusters are opaque with a thickness on the order of 10^2 μm^3, while the thickness is generally on the order of 10^4 μm for spectral emittance measurements, which means that τ has little effect on the char/ash particle cluster spectral emittance. However, the spectral emittance was affected by τ for spectral emittance measurements of suspended semi-transparent char/ash particle clouds[38]. The mineral content and coal rank then affect τ and thus, the spectral emittance and unburned carbon concentration measurements. Therefore, the optically opaque nature of char/ash

	SiO$_2$/%	Al$_2$O$_3$/%	CaO/%	Fe$_2$O$_3$/%
Shenhua	56.83	26.17	10.20	6.98
Yankuang	44.50	35.00	13.02	7.48

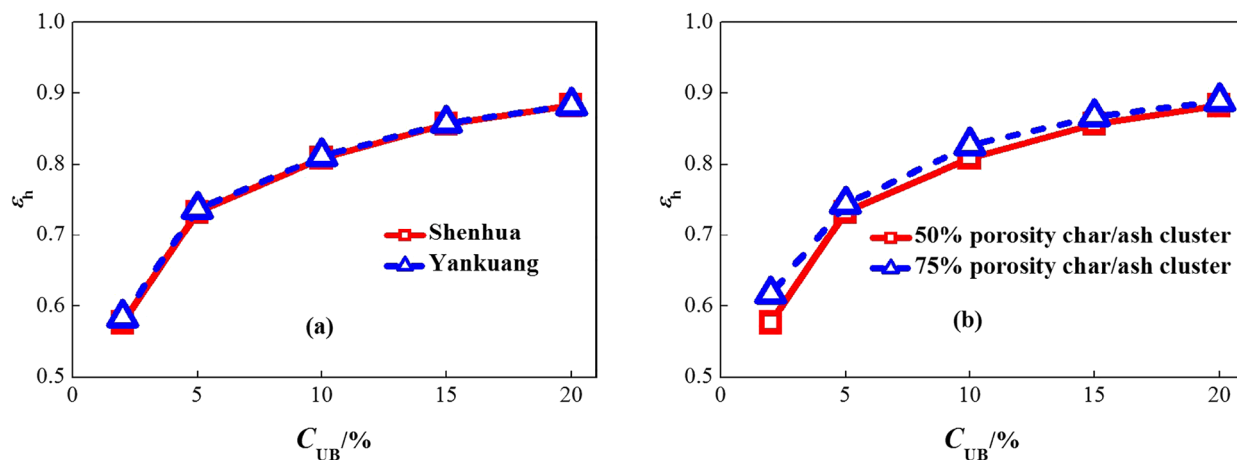**Table 1 | Mineral content of Shenhua and Yankuang coal fly ash**

Figure 2 | Effects of (a) mineral content and (b) coal rank (the two porosities represent different coal ranks) on the spectral emittance.

particle clusters is the first reason that the mineral content and coal rank have little effect on the unburned carbon concentration measurements. Char and ash are both strongly forward scattering particles[46] regardless of the mineral content or coal ranks. Therefore, the mineral content and coal rank have little effect on $\Phi(\mu, \mu')$ and, thus, on the spectral emittance and unburned carbon concentration measurements.

Since the optical depth and phase function have little effect, the char/ash particle cluster spectral emittance is only affected by the scattering albedo, which is further seen in the similar trends of the $\varepsilon_h \sim \lambda$ and $(1 - \omega) \sim \lambda$ curves plotted in figure 3(a). $1 - \omega$ characterizes the ratio of the absorption efficiency to the extinction efficiency. Therefore, measurements of the char/ash particle cluster spectral emittance are actually relative measurements, unlike the absolute measurements of the transmission power in the microwave absorption method[32,33], the reflected light intensity in the optical dispersion-reflection method[34,35], and the atomic emission signal in the laser-induced breakdown spectroscopy method[36,37]. The similar trends in the $\kappa \sim \lambda$ and $(1 - \omega) \sim \lambda$ curves plotted in figure 3(b) show that the absorption index, κ, is the dominant effect to determine the ratio of the absorption efficiency to the extinction efficiency, and, thus, the cluster spectral emittance. Given that the absorption index of carbon is three orders of magnitude higher than that of pure ash at wavelengths below 4 μm, the char/ash particle cluster spectral emittance at short wavelengths is sensitive to the unburned carbon concentrations and insensitive to the mineral content and coal rank. The fly ash cluster spectral emittance has been measured on-line by Moore et al.[47]. Therefore, this paper provides implications that the char/ash particle cluster spectral emittance method is a promising route for unburned carbon concentration

on-line measurements that is independent of the mineral content and coal rank effects.

Discussion

This paper describes the char/ash particle cluster spectral emittance method for unburned carbon concentration measurements. The effects of mineral content and coal rank were investigated to determine their influence on the spectral emittance measurements. The spectral emittance was found to be sensitive to the unburned carbon concentrations and insensitive to mineral content and coal rank at short wavelengths due to the optically thick and strong forward scattering nature of char/ash particle clusters, and the fact that the absorption index of carbon is three orders of magnitude higher than that of pure ash at short wavelengths. This paper provides implications that the char/ash particle cluster spectral emittance method described here is a novel and promising route for on-line unburned carbon concentration measurements that is not influenced by mineral content and coal rank effects.

Methods

A char/ash particle cluster is modeled as an isothermal, one-dimensional, equivalent homogeneous semitransparent absorbing and scattering layer. The radiative transfer equation is[48]:

$$\mu \frac{\partial I(\tau,\mu)}{\partial \tau} = (1-\omega)I_b - I(\tau,\mu) + \frac{\omega}{2}\int_{-1}^{1}\Phi(\mu,\mu')I(\tau,\mu')\mathrm{d}\mu' \qquad (1)$$

where τ is the optical depth, $I(\tau,\mu)$ is the radiation intensity at position τ and direction μ ($=\cos\theta$, where θ is the angle between the direction and the positive τ direction), I_b is the radiation intensity emitted by the blackbody at the cluster temperature, ω ($=Q_s/Q_e$, where Q_s is the scattering efficiency and Q_e is the extinction efficiency) is the scattering albedo and $\Phi(\mu, \mu')$ is the phase function.
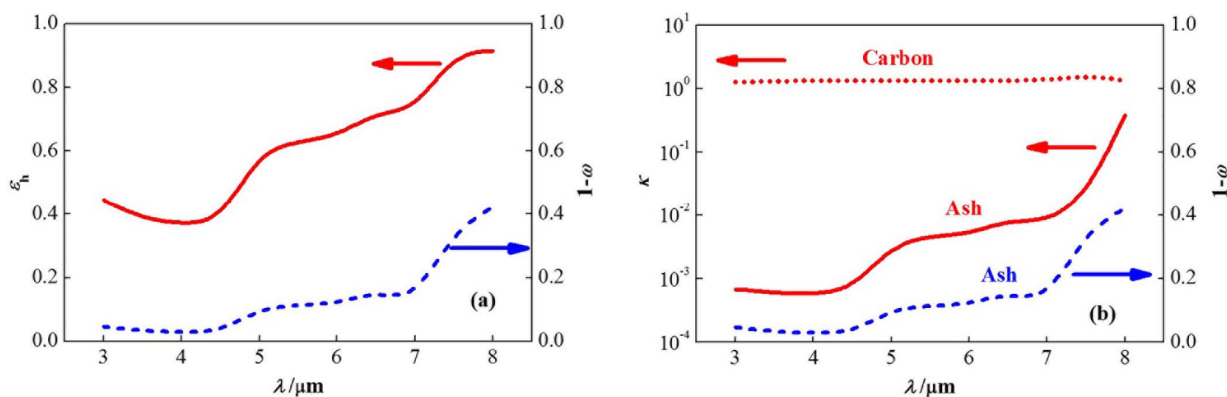

Figure 3 | (a) Spectral emittance and (b) Absorption index change with scattering albedo.

The radiative transfer equation was solved using the S-12 discrete ordinate method[49] with equation (1) then converted to 24 differential equations, one for each transfer direction, expressed as:

$$\mu_i \frac{\partial I(\tau,\mu_i)}{\partial \tau} = (1-\omega)I_b - I(\tau,\mu_i) + \frac{\omega}{2}\sum_{j=1}^{24} W_j \Phi(\mu_i,\mu_j) I(\tau,\mu_j) \qquad (2)$$

The boundary conditions are:

$$I(0,\mu>0)=0 \qquad (3)$$

$$I(\tfrac{1}{2}\tau_{max},\mu)=I(\tfrac{1}{2}\tau_{max},-\mu) \qquad (4)$$

Combining of equations (2)–(4) gives the hemispherical emittance, ε_h, as:

$$\varepsilon_h = \frac{\sum_{i=1}^{24} W_i I(\tau_{max},\mu>0)}{\sum_{i=1}^{24} W_i I_b} \qquad (5)$$

Fiveland[49] gave details on how to solve equation (2).

The radiative transfer equation model requires knowledge of the scattering albedo and the phase function to calculate the char/ash particle cluster emittance using equation (5). Three common cluster radiative property computation methods are the multiple sphere T-matrix, discrete dipole approximation (DDA) and generalized multiparticle Mie-solution (GMM). The T-matrix method relies on more accurate equations for every particle's optical cross-sections than the DDA method, and is capable of multi-processor parallelization that is not possible with the GMM method[50]. Therefore, the multiple sphere T-matrix method was implemented in the open source code by Mackowski and Mishchenko[50] to accurately calculate the cluster radiative properties.

The T-matrix method uses the size parameter x ($=\pi D/\lambda$, where D is the particle diameter and λ is the wavelength), optical constants m ($=n + \kappa i$, where n is the refractive index and κ is the absorption index) and position profiles of each particle in the cluster. This algorithm has several steps[50]: (1) Determine each particle's individual scattering parameters using Mie theory as expansions of the vector spherical wave functions (VSWF). (2) Use the extended boundary condition method (EBCM) to calculate the relationships between the expansion coefficients for different particles as a set of linear equations. (3) Iteratively solve the resulting equations until the residual satisfies the required error limit. (4) Use the scattering from all the particles to calculate the radiative parameters of each particle.

Representative aggregates were generated to provide realistic particle geometric distributions in the char/ash clusters for the T-matrix calculations. These aggregates are representative of actual char/ash particle clusters in terms of the particle size, porosity and unburned carbon concentration. Representative aggregates were first generated for high rank bituminous and anthracite coals. The coal rank effect was then analyzed in the results and discussion section.

The fly ash carbon has been found to be distributed in discrete carbon-rich char particles[51], so the representative aggregates included carbon-free ash particles and carbon-rich char particles. The ash and char particles have been found to have similar size distributions for high rank coals[52]. The effect of the particle size distribution has

been determined by comparing the spectral emittance calculated using Mie theory for ash clusters with uniform diameters and with lognormal size distributions[3]. This effect was found to cause average relative differences of less than 3%. Therefore, the ash and char particles were assumed to have one uniform diameter.

Hurt et al.[44,45] analyzed carbon-rich extracts from the fly ash mineral content of eight types of coal to show that these extracts had a typical carbon concentration of 75%. In addition, the unburned carbon content has a dominant maceral component of inertinite[53] with 50% porosity[43]. Therefore, each char particle was assumed to be a 50% porosity sphere consisting of 25% ash and 75% carbon. The Maxwell-Garnett effective medium theory[3,44] was used to determine the ash and char particle optical constants from the chemical compositions. The representative aggregates were generated using the open-source code by Bentz[55]. The particles were first randomly placed in a cube and then each particle walked randomly until it contacted and adhered to another particle. The numbers of ash and char particles were determined by the unburned carbon concentrations and particle volume fractions.

Figure 4 shows the calculated spectral emittance of representative 524 and 1114 particle aggregates generated using the Bentz method and a 524 particle aggregate generated using the diffusion-limited aggregation (DLA) method[56] for a char/ash particle cluster with 9 µm diameter, 0.2 particle volume fraction and 2% unburned carbon concentration. The optical constants were taken from Goodwin and Mitchner[57] for the mineral content, SiO_2, Fe_2O_3, Al_2O_3, CaO and MgO, and from Foster and Howarth[58] for the carbon. These results agree well with each other which means that the 524 particle aggregate is representative of the char/ash particle cluster and that the different random aggregation algorithms have little effect on the cluster radiative properties.

Further validation of the theoretical method and results is provided in the Supplementary Information.

1. Ahmaruzzaman, M. A review on the utilization of fly ash. *Prog. Energ. Combust. Sci.* **36**, 327–363 (2010).
2. Somers, C. M., McCarry, B. E., Malek, F. & Quinn, J. S. Reduction of Particulate Air Pollution Lowers the Risk of Heritable Mutations in Mice. *Science* **304**, 1008–1010 (2004).
3. Liu, D., Duan, Y. Y., Yang, Z. & Yu, H. T. Theoretical predictions of spectral emissivity for coal ash deposits. *ASME J. Heat Trans* 2013. (In press).
4. Liu, D., Duan, Y. Y. & Yang, Z. Effects of wake dynamics on infrared measurements of particle cloud temperatures in the superheater pendant region of utility boilers. *Appl. Therm. Eng.* **51**, 1076–1081 (2013).
5. Liu, D., Duan, Y. Y. & Yang, Z. Calculations of the average normal effective emissivity for nonaxisymmetric cavities using the modified finite volume method. *Opt. Eng.* **52**, 039702 (2013).
6. Liu, D., Duan, Y. Y. & Yang, Z. Integrated effective emissivity computation for non-isothermal non-axisymmetric cavities. *Chin. Opt. Lett.* **11**, 022001 (2013).
7. Liu, D., Duan, Y. Y. & Yang, Z. Effects of participating media on the time-resolved infrared measurements of wall temperature in a coal-fired combustor. *Exp. Therm. Fluid Sci.* **39**, 90–97 (2012).
8. Hower, J. C. *et al.* Mercury capture by native fly ash carbons in coal-fired power plants. *Prog. Energ. Combust. Sci.* **36**, 510–529 (2010).
9. Zheng, Y. J., Jensen, A. D., Windelin, C. & Jensen, F. Review of technologies for mercury removal from flue gas from cement production processes. *Prog. Energ. Combust. Sci.* **38**, 599–629 (2012).
10. Maroto-Valer, M. M., Lu, Z., Zhang, Y. Z. & Tang, Z. Sorbents for CO_2 capture from high carbon fly ashes. *Waste Manage.* **28**, 2320–2328 (2008).
11. Li, F. X. & Fan, L. S. Clean coal conversion processes - progress and challenges. *Energ. Environ. Sci.* **1**, 248–267 (2008).
12. Wang, Q., Luo, J. Z., Zhong, Z. Y. & Borgna, A. CO_2 capture by solid adsorbents and their applications current status and new trends. *Energ. Environ. Sci.* **4**, 42–55 (2011).
13. Su, F. S. & Lu, C. CO_2 capture from gas stream by zeolite 13× using a dual-column temperature/vacuum swing adsorption. *Energ. Environ. Sci.* **5**, 9021–9027 (2012).
14. Akhtar, F., Liu, Q. L., Hedin, N. & Bergstrom, L. Strong and binder free structured zeolite sorbents with very high CO_2-over-N_2 selectivities and high capacities to adsorb CO_2 rapidly. *Energ. Environ. Sci.* **5**, 7664–7673 (2012).
15. Bae, T. H. *et al.* Evaluation of cation-exchanged zeolite adsorbents for post-combustion carbon dioxide capture. *Energ. Environ. Sci.* **6**, 128–138 (2013).
16. Liu, Q. *et al.* Adsorption of carbon dioxide by MIL-101(Cr): regeneration conditions and influence of flue gas contaminants. *Sci. Rep.* **3**, 2916 (2013).
17. Li, Y. C., Yan, Q. J., Kong, C. L. & Chen, L. Polyethyleneimine incorporated metal-organic frameworks adsorbent for highly selective CO2 capture. *Sci. Rep.* **3**, 1859 (2013).
18. Davini, P. Flue gas treatment by activated carbon obtained from oil-fired fly ash. *Carbon* **40**, 1973–1979 (2002).
19. Li, J. R. & Maroto-Valer, M. M. Computational and experimental studies of mercury adsorption on unburned carbon present in fly ash. *Carbon* **50**, 1913–1924 (2012).
20. Tan, Z. Q. *et al.* Gas-phase elemental mercury removal by novel carbon-based sorbents. *Carbon* **50**, 362–371 (2012).
21. Yan, N. Q. *et al.* Enhanced elemental mercury removal from coal-fired flue gas by sulfur−chlorine compounds. *Environ. Sci. Technol.* **43**, 5410–5415 (2009).
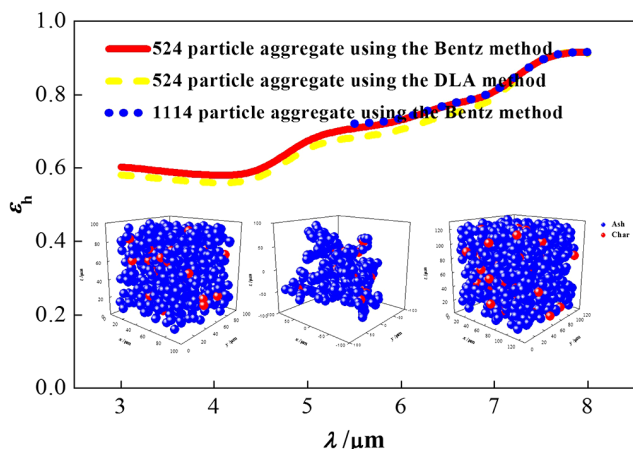
Figure 4 | Spectral emittance of various representative aggregates. The left inset is the 524 particle aggregate generated using the Bentz method, the middle one is a 524 particle aggregate generated using the DLA method, and the right one is an 1114 particle aggregate generated using the Bentz method.

22. Qu, Z., Yan, N. Q., Liu, P., Guo, Y. F. & Jia, J. P. Oxidation and stabilization of elemental mercury from coal-fired flue gas by sulfur monobromide. *Environ. Sci. Technol.* **44**, 3889–3894 (2010).

23. Tong, S. T., Fan, M. X., Mao, L. & Jia, Q. Sequential extraction study of stability of adsorbed mercury in chemically modified activated carbons. *Environ. Sci. Technol.* **45**, 7416–7421 (2011).

24. Bisson, T. M., MacLean, L. C. W., Hu, Y. F. & Xu, Z. H. Characterization of mercury binding onto a novel brominated biomass ash sorbent by X-ray absorption spectroscopy. *Environ. Sci. Technol.* **46**, 12186–12193 (2012).

25. Clack, H. L. Estimates of increased black carbon emissions from electrostatic precipitators during powdered activated carbon injection for mercury emissions control. *Environ. Sci. Technol.* **46**, 7327–7333 (2012).

26. Pattanayak, J., Mondal, K., Mathew, S. & Lalvani, S. B. A parametric evaluation of the removal of As(V) and As(III) by carbon-based adsorbents. *Carbon* **38**, 589–596 (2000).

27. Chingombe, P., Saha, B. & Wakeman, R. J. Surface modification and characterisation of a coal-based activated carbon. *Carbon* **43**, 3132–3143 (2005).

28. Zhu, J. Z., Deng, B. L., Yang, J. & Gang, D. C. Modifying activated carbon with hybrid ligands for enhancing aqueous mercury removal. *Carbon* **47**, 2014–2025 (2009).

29. Sakthivel, T., Reid, D. L., Goldstein, I., Hench, L. & Seal, S. Hydrophobic high surface area zeolites derived from fly ash for oil spill remediation. *Environ. Sci. Technol.* **47**, 5843–5850 (2013).

30. Fan, M. H. & Brown, R. C. Precision and accuracy of photoacoustic measurements of unburned carbon in fly ash. *Fuel* **80**, 1545–1554 (2001).

31. Pandhija, S., Rai, N. K., Singh, A. K., Rai, A. K. & Gopal, R. Development of photoacoustic spectroscopic technique for the study of materials. *Prog. Cryst. Growth. Charact. Mater.* **52**, 53–60 (2006).

32. Smith, K., Dixon, T. & Taylor, J. On-line monitoring of carbon in fly ash for boiler control. *2009 World of Coal Ash (WOCA) Conference*.

33. Liu, H. Y., Tan, H. Z., Gao, Q., Wang, X. B. & Xu, T. M. Microwave attenuation characteristics of unburned carbon in fly ash. *Fuel* **89**, 3352–3357 (2010).

34. Styszko-Grochowiak, K., Golas, J., Jankowski, H. & Kozinski, S. Characterization of the coal fly ash for the purpose of improvement of industrial on-line measurement of unburned carbon content. *Fuel* **83**, 1847–1853 (2004).

35. Xu, H. W., Zhou, H. & Cen, K. F. Measure carbon content in fly ash by infrared reflection method. *J. Zhejiang Univ. Eng. Sci.* **45**, 890–895 (2011). (In Chinese).

36. Zhang, L. *et al.* Development of an apparatus for on-line analysis of unburned carbon in fly ash using laser-induced breakdown spectroscopy (LIBS). *Appl. Spectrosc.* **65**, 790–796 (2011).

37. Yao, S. C., Lu, J. D., Zheng, J. P. & Dong, M. R. Analyzing unburned carbon in fly ash using laser-induced breakdown spectroscopy with multivariate calibration method. *J. Anal. At. Spectrom.* **27**, 473–478 (2012).

38. Bonanno, A. S., Knight, K. S., Kinsella, K., Serio, M. A. & Solomon, P. R. In-situ measurement of residual carbon content in flyash. *Proc. SPIE* **2367**, 194–201 (1995).

39. Lou, C., Zhou, H. C., Yu, P. F. & Jiang, Z. W. Measurements of the flame emissivity and radiative properties of particulate medium in pulverized-coal-fired boiler furnaces by image processing of visible radiation. *P. Combust. Inst.* **31**, 2771–2778 (2007).

40. Li, G. D. *et al.* Comparison of particulate formation and ash deposition under oxy-fuel and conventional pulverized coal combustions. *Fuel* **106**, 544–551 (2013).

41. Bhattacharya, S. P. & Wall, T. F. Development of emittance of coal particles during devolatilisation and burnoff. *Fuel* **78**, 511–519 (1999).

42. Xu, X. G., Li, S. Q., Li, G. D. & Yao, Q. Effect of co-firing straw with two coals on the ash deposition behavior in a down-fired pulverized coal combustor. *Energ. Fuel* **24**, 241–249 (2010).

43. Yu, J. L., Lucas, J. A. & Wall, T. F. Formation of the structure of chars during devolatilization of pulverized coal and its thermoproperties: a review. *Prog. Energy. Combust. Sci.* **33**, 135–170 (2007).

44. Hurt, R. H. & Gibbins, J. R. Residual carbon from pulverized coal fired boilers: 1. size distribution and combustion reactivity. *Fuel* **74**, 471–480 (1995).

45. Hurt, R. H., Davis, K. A., Yang, N. Y. C., Headley, T. J. & Mitchell, G. D. Residual carbon from pulverized-coal-fired boilers: 2. morphology and physicochemical properties. *Fuel* **74**, 1297–1306 (1995).

46. Itaya, Y. *et al.* Thermal radiation characteristics of coal char ash particles dispersed in a gasification furnace. *J. Chem. Eng. Jpn.* **37**, 1367–1372 (2004).

47. Moore, T. J. *et al.* In situ measurements of the spectral emittance of coal ash deposits. *J. Quant. Spectrosc. Ra.* **112**, 1978–1986 (2011).

48. Liemert, A. & Kienle, A. Exact and efficient solution of the radiative transport equation for the semi-infinite medium. *Sci. Rep.* **3**, 2018 (2013).

49. Fiveland, W. A. Discrete ordinate methods for radiative heat-transfer in isotropically and anisotropically scattering media. *ASME J. Heat Trans.* **109**, 809–812 (1987).

50. Mackowski, D. W. & Mishchenko, M. I. A multiple sphere T-matrix Fortran code for use on parallel computer clusters. *J. Quant. Spectrosc. Ra.* **112**, 2182–2192 (2011).

51. Kulaots, I., Hurt, R. H. & Suuberg, E. M. Size distribution of unburned carbon in coal fly ash and its implications. *Fuel* **83**, 223–230 (2004).

52. Lu, Y. Q., Rostam-Abadi, M., Chang, M. Richardson, C. & Paradis, J. Characteristics of fly ashes from full-scale coal-fired power plants and their relationship to mercury adsorption. *Energ. Fuel* **21**, 2112–2120 (2007).

53. Sharonova, O. M., Anshits, N. N., Yumashev, V. V. & Anshits, A. G. Composition and morphology of char particles of fly ashes from industrial burning of high-ash coals with different reactivity. *Fuel* **87**, 1989–1997 (2008).

54. Bohren, C. F. & Huffman, D. R. *Absorption and Scattering of Light by Small Particles*, Wiley, New York (1983).

55. Bentz, D. P. Three-dimensional computer simulation of cement hydration and microstructure development. *J. Amer. Ceram. Soc.* **80**, 3–21 (1997).

56. Lallich, S., Enguehard, F. & Baillis, D. Experimental determination and modeling of the radiative properties of silica nanoporous matrices. *ASME J. Heat Trans.* **131**, 082701 (2009).

57. Goodwin, D. G. & Mitchner, M. Infrared optical constants of coal slags: dependence on chemical composition. *J. Thermophys. Heat Trans.* **3**, 53–60 (1989).

58. Foster, P. J. & Howarth, C. R. Optical constants of carbons and coals in the infrared. *Carbon* **6**, 719–729 (1968).

Acknowledgments

Author contributions

D.L., Y.D. and Z.Y. designed the project. D.L. and H.Y. calculated the spectral emittance. D.L. wrote the manuscript. All authors discussed the results and commented on the manuscript.

Additional information